A&A 669, L16 (2023)
https://doi.org/10.1051/0004-6361/202245576

Astronomy & Astrophysics
Special issue

Solar Orbiter First Results (Nominal Mission Phase)

LETTER TO THE EDITOR

The 18–19 March 2022 series of ^{3}He-rich events observed by Solar Orbiter at 0.36 au compared with EUV, X-ray, and radio observations⋆

G. M. Mason[1], N. V. Nitta[2], R. Bučík[3], R. Gómez-Herrero[4], V. Krupar[5,6], S. Krucker[7,8], G. C. Ho[1], R. C. Allen[1], A. Kouloumvakos[1], R. F. Wimmer-Schweingruber[9], J. Rodriguez-Pacheco[4], A. Vecchio[10,11], and M. Maksimovic[11]

[1] Johns Hopkins Univ. Applied Physics Laboratory, 11100 Johns Hopkins Rd., Laurel, MD, USA
e-mail: Glenn.Mason@jhuapl.edu
[2] Lockheed Martin Advanced Technology Center, Dept/A021S, B/252, 3251 Hanover Street, Palo Alto, CA 94304, USA
[3] Southwest Research Institute, 6220 Culebra Road, Sal Antonio, TX 78238, USA
[4] Universidad de Alcalá, Space Research Group, 28805 Alcalá de Henares, Madrid, Spain
[5] Goddard Planetary Heliophysics Institute, University of Maryland, Baltimore County, Baltimore, MD 21250, USA
[6] Heliophysics Science Division, NASA Goddard Space Flight Center, 8800 Greenbelt Rd, Greenbelt, MD, USA
[7] University of Applied Sciences and Arts Northwestern Switzerland, 5210 Windisch, Switzerland
[8] Space Sciences Laboratory, University of California, 7 Gauss Way, Berkeley, CA 94720, USA
[9] Institut für Experimentelle und Angewandte Physik, Christian-Albrechts-Universität zu Kiel, Leibnizstrasse 11, Kiel, Germany
[10] Radboud Radio Lab – Department of Astrophysics, Radboud University, Nijmegen, The Netherlands
[11] LESIA, Observatoire de Paris, Universite PSL, CNRS, Sorbonne Universite, Universite de Paris, 5 Place Jules Janssen, 92195 Meudon, France

Received 29 November 2022 / Accepted 29 December 2022

ABSTRACT

Context. During the first close perihelion pass of Solar Orbiter, a series of impulsive ^{3}He-rich solar particle events was observed on 18–19 March 2022 from a distance of 0.36 au. In addition to the energetic particle, radio, and X-ray data from Solar Orbiter, the events were observed in radio and/or extreme ultraviolet by STEREO-A, SDO, Wind, and Parker Solar Probe.
Aims. Observations of the event series along with remote sensing of flaring and radio emission with only small timing delays due to the close distance allow the association with energetic particles to be determined with much higher accuracy than previously possible from 1 au.
Methods. By comparing the onsets of type-III bursts with the arrival of electrons of tens of keV at Solar Orbiter only a few minutes later, it can be seen that, overall, each of the more intense type-III bursts was associated with an electron and ion injection. Extreme ultraviolet data show that the times of the type-III bursts coincide with emission from a small (approximately Earth-sized) loop to the west of a nearby active region.
Results. The energetic particle spectra and abundances show typical properties of impulsive ^{3}He-rich flares and, when combined with the remote sensing observations, establish that the particle-accelerating mechanism in this series of events operates near the solar surface in association with magnetic loops, and in the absence of other phenomena such as jets and small coronal mass ejections.

Key words. acceleration of particles – Sun: flares – Sun: particle emission – Sun: radio radiation – Sun: UV radiation – Sun: X-rays, gamma rays

1. Introduction

One of the major goals of the Solar Orbiter mission is to understand how energetic particles are accelerated at the Sun and then released from their sources into interplanetary space (Müller et al. 2020). Energetic-particle-producing events at the Sun fall into two broad classes, namely large events associated with coronal mass ejections (CMEs) and smaller, "impulsive" events rich in electrons, heavy ions, and the rare isotope ^{3}He (see, e.g., reviews by Desai & Giacalone 2016; Reames 1999, 2017). While impulsive events occur by the thousands in active portions of the solar cycle, the relation between particle events and microflares is mostly established by statistics (Wang et al. 2012) due to the large distance to the source. By traveling closer to the Sun and thereby lessening the effects of interplanetary mixing, connectivity, and timing, the coordinated observations from Solar Orbiter can untangle processes in a way not possible near 1 au. In this Letter we present novel insights into impulsive solar energetic particle (SEP) events obtained during the first close perihelion pass of Solar Orbiter, which were observed with unprecedented detail.

2. Observations

The energetic particle observations discussed here are from the Solar Orbiter Energetic Particle Detector (EPD) suite

⋆ Movie associated to Fig. 4 is available at https://www.aanda.org

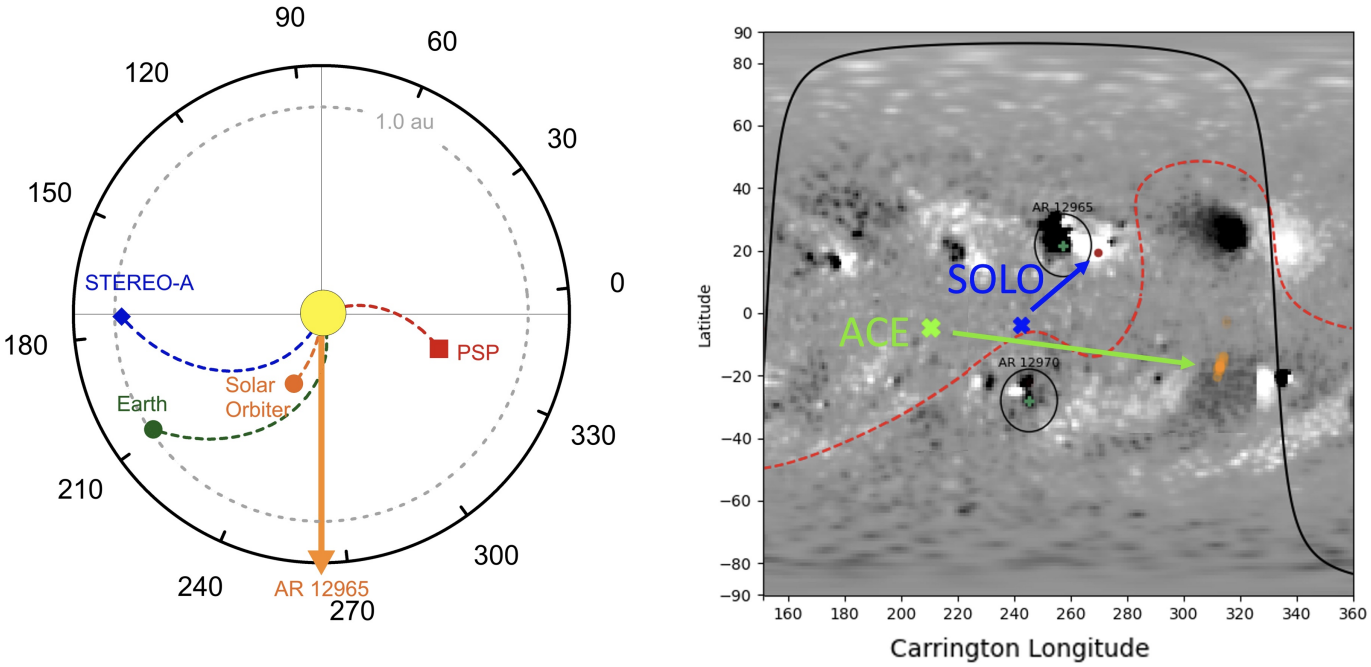

Fig. 1. Overview of spacecraft constellation and solar regions. *Left*: spacecraft locations in Carrington longitude and heliocentric radius at 00:00 on 19 March 2022. Magnetic spirals use the measured solar wind speed at each location. The arrow marks the longitude of AR 12965. *Right*: calculated magnetic connections for Solar Orbiter and Earth (ACE; see text for details). The dashed red line is the heliospheric current sheet.

(Rodríguez-Pacheco et al. 2020; Wimmer-Schweingruber et al. 2021). Radio wave data are from the Solar Orbiter Radio and Plasma Wave investigation (RPW; Maksimovic et al. 2020), X-ray data from the Solar Orbiter Spectrometer/Telescope for Imaging X-rays (STIX; Krucker et al. 2020), and extreme ultraviolet (EUV) data from the Atmospheric Imaging Assembly (AIA; Lemen et al. 2012) on the Solar Dynamics Observatory (SDO). Figure 1 (left) shows spacecraft positions in the period of interest when emissions took place from or near active region (AR) 12965, which is located at N25W55 (Carrington longitude 264). The right panel of the figure shows subsolar points for Solar Orbiter (blue) and Earth (Advanced Composition Explorer, ACE, green) and arrows pointing to the connection sites on the solar surface calculated with a tool that incorporates solar wind speed and Potential Field Source Surface (PFSS) modeling (see Rouillard et al. 2020). Solar Orbiter is connected on the west side of AR 12965 and remained so throughout the 18–19 March period. It should be noted that Earth, although seemingly connected nearby Solar Orbiter in the left panel, is in fact connected 40–50° away and on the other side of the current sheet. The Solar Terrestrial Relations Observatory-A spacecraft (STEREO-A, not shown) was connected away from the Solar Orbiter point most of the time. Neither ACE nor STEREO-A He intensities showed obvious increases during this period.

2.1. Energetic particle and radio observations

Figure 2 shows an overview of the observations. The top panel shows heavy ion ($m > 10$ amu) arrival times from the EPD/Suprathermal Ion Spectrograph (SIS), where each dot is an individual ion. The slanted line at the left of the panel shows the slope of arrival times at 0.36 au, assuming pure velocity dispersion for a Parker spiral and a 400 km s^{-1} solar wind speed. The ion pattern shows multiple events, arriving with slopes close to the velocity dispersion line. Vertical features, before event 5 and near events 13 and 15, are dispersion-less temporary enhancements due to interplanetary field line mixing, which modulates the intensities and sometimes causes dropouts (e.g., Chollet et al. 2009; Ho et al. 2022; Mazur et al. 2000). The middle panel shows arrival times for electrons from the EPD/Electron Proton Telescope (EPT) and SupraThermal Electrons and Protons Telescope (STEP). Near the middle of the energy range in the respective panels, the flight time for ions is ~3 h, while for electrons it is ~8 min. The lower panel shows radio data from RPW, with a series of type-III bursts.

The energetic particle events have a clear association with the onset and ending of the type-III burst series, with extremely low particle activity before the series starts at around 09:00 on 18 March 2022 and after it ends at around 07:00 on 19 March 2022. Dotted lines in the figure connect the onsets of prominent type-III bursts with the electron events, and then to the ion events whose slower particles arrive over several hours in each case. There are about 15 ion events discernable, with all but event 8 plausibly associated with a type-III burst and electron event. It is interesting that the type IIIs with correspondence to the particle events are generally those that extend to frequencies below ~0.1 MHz. The Geostationary Operational Environmental Satellites (GOES) satellites reported a number of B- and C-class X-ray events during this period (red arrows at the top) whose timing is close to some of the type-III burst times, but there are fewer events.

Figure 3 examines a 3 h sub-period to better illustrate the associations between particle and radio emissions. The type IIIs at ~22:12 and 23:17 correspond to events 9 and 10 in Fig. 2. The correspondence between the type-III onsets and extrapolated c/v electron spectrograms is very close. The 23:17 type III has a faint second injection that may correspond to the double injection of electrons, which is not resolvable with the much slower ions. The ghost-like type III at ~21:21 might correspond to event 8 in Fig. 2 but is not visible on the larger scale because there were some intense type-III bursts (events 2 and 3) at the beginning of the longer period that change the color scale of the spectrogram.

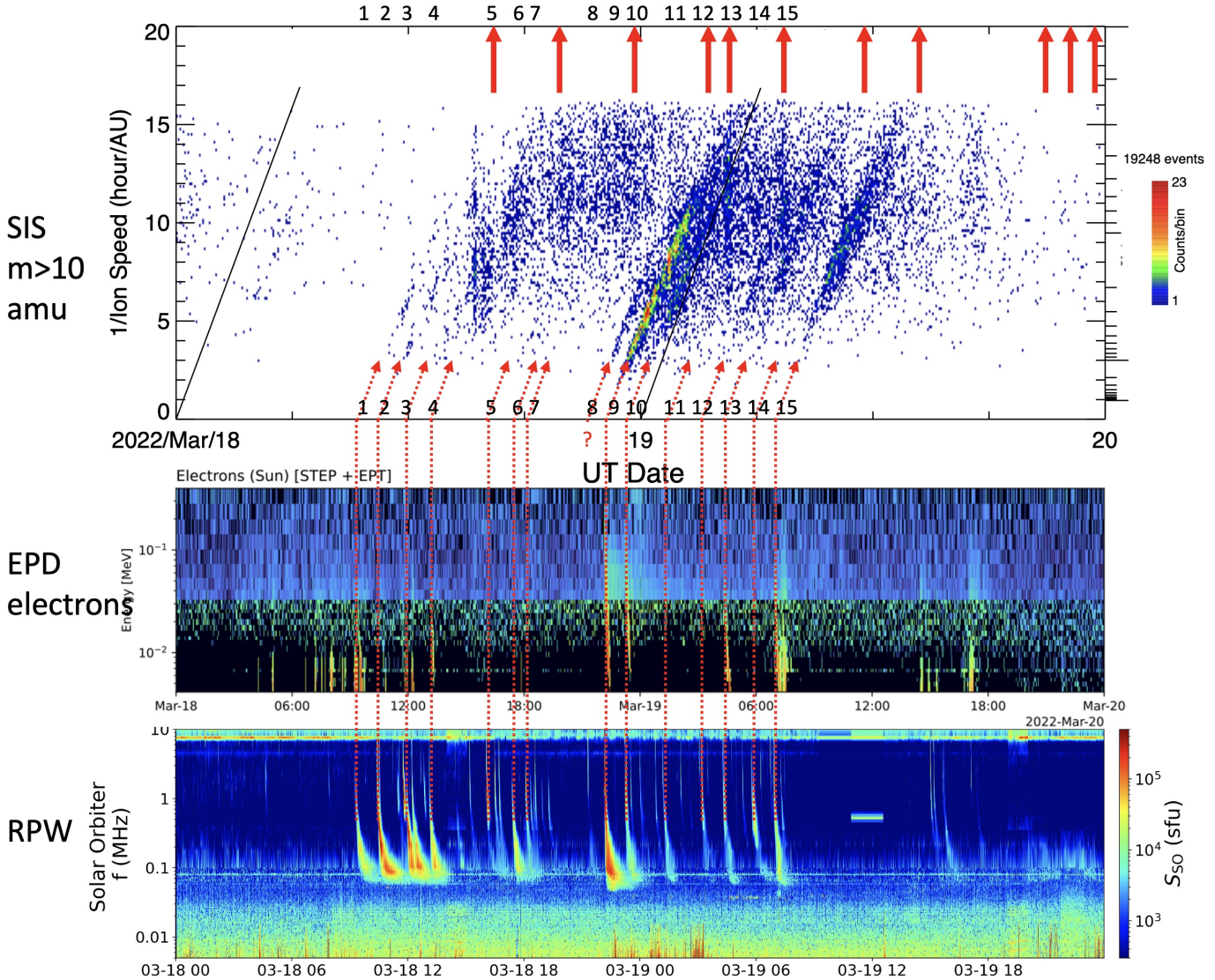

Fig. 2. Overview of the period. *Top panel*: 10–70 amu individual ion 1/speed vs. arrival time at Solar Orbiter; red arrows mark times of GOES 1–8 Å B- and C-class flares. *Middle panel*: electron spectrograms at Solar Orbiter. *Bottom panel*: RPW type-III radio bursts. See text for discussion.

In the lower panel, STIX X-rays show a small increase around event 9. Near the end of the period, but after event 10, there was an X-ray rise classified as a B7.1 event on the U.S. National Oceanic and Atmospheric Administration (NOAA) list, starting at 23:30 from AR 12965. STIX imaging locates this event near AR 12965, as shown in the solar map (view from Solar Orbiter).

2.2. Source of the activity

In order to estimate the source of the type IIIs, we used radio observations from Solar Orbiter, Parker Solar Probe (PSP), STEREO-A, and Wind, which viewed AR 12965 from different directions and distances (Fig. 1). Applying a cyclic Gauss fitting to the intensity peaks at six frequencies between 434 and 1013 kHz, we obtain a mean location of 44.3 ± 3.8° from the central meridian, reasonably close to the AR. A movie of SDO AIA 94 Å between 21:00 and 24:00 on 18 March revealed a small loop (Fig. 4) that brightened in coincidence with events 8, 9, and 10 in Fig. 3. The brightening lasted a few minutes in each case. During this period there were no obvious jets, and the AR to the left in the figure was reasonably quiet. At the start of the B7.1 event, loops in the AR brightened significantly. The movie is available online.

2.3. Energetic particle spectra and composition

Figure 5 shows energetic particle spectra from Solar Orbiter/SIS for event 9. These spectra were formed by varying the collection time as a function of energy so that only particles in the slanted burst in Fig. 2 are included (see details in Mason et al. 2000). Above 0.1–0.2 MeV nucleon^{-1}, the spectral shapes are similar for different species. Although somewhat curved, the ^{4}He spectrum above ~0.25 MeV nucleon^{-1} is reasonably well fitted by a power law with exponent −3.5. The O and Fe spectra are much harder but soften at higher energies around 1 MeV nucleon^{-1}. The inset to Fig. 5 shows a histogram of 0.5–2.0 MeV nucleon^{-1} He, which shows a ratio of ^{3}He:^{4}He = 0.04 ± 0.01. This is a modest enrichment for a ^{3}He-rich event but is ~100 times larger than

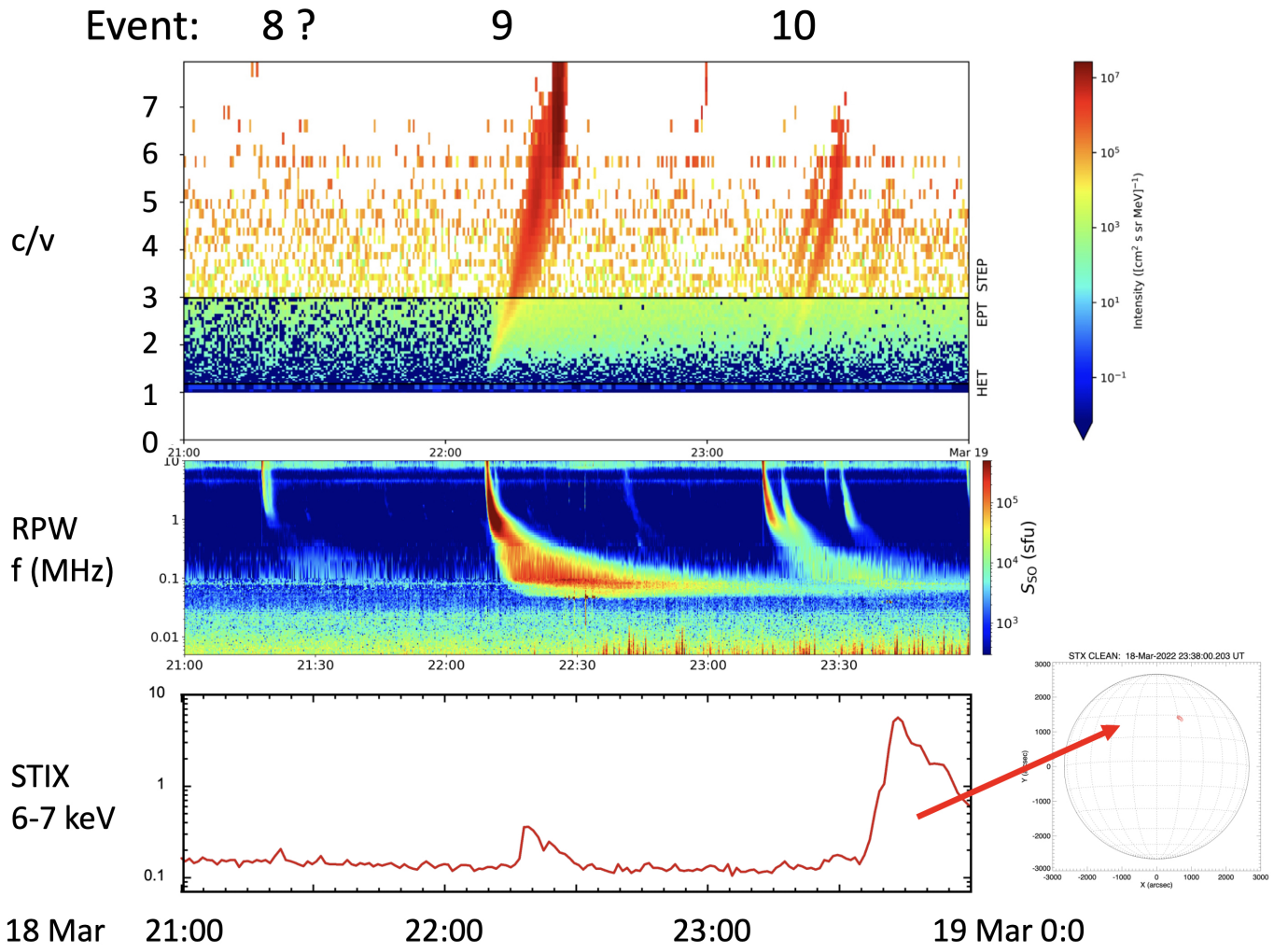

Fig. 3. Expanded period at the end of 18 March. *Top panel*: electron c/speed vs. arrival time at Solar Orbiter for events 8–10 in Fig. 2. *Middle panel*: RPW radio data. *Lower panel*: STIX X-ray intensity and location of a larger event near AR 12965 that occurred at the end.

the slow solar wind value of $(4.08 \pm 0.25) \times 10^{-4}$ (Bodmer et al. 1995; Gloeckler & Geiss 1998). The heavy ion composition over the range 320–450 keV nucleon^{-1} for event 9 is shown in Fig. 6, where it is compared with the 20-event survey of Mason et al. (2004) over the same range and the Reames (1999) survey at ~2.5 MeV nucleon^{-1}; it shows that the event 9 composition is comparable to other ^{3}He-rich events for C and heavier ions. The H and ^{4}He values are much lower than the survey averages.

2.4. Anisotropies

Particle anisotropies for the period can be estimated from Fig. 7, which plots 30-min-averaged 273 keV nucleon^{-1} H and ^{3}He intensities for the Solar Orbiter/SIS telescopes, which point at 30° ("sunward") and 160° ("anti-sunward") west from the spacecraft–Sun line. The sunward telescope samples close to the average interplanetary magnetic field (IMF) direction, while the anti-sunward telescope samples particles moving toward the Sun. Unlike the heavy ions, the proton intensity is elevated at the beginning of the period due to prior activity and then decays slowly with the ^{3}He events superposed above it. The ^{3}He intensity is extremely low except during the peak, which corresponds to event 9. In this format, which examines a narrow energy band, the distinction between different events shown in Fig. 2 is washed out. We note that the H and ^{3}He peak at the same time. At the peak, the sunward/anti-sunward intensity ratios are >20:1.

3. Discussions and conclusions

The 18–19 March 2022 series of events were observed with unprecedented detail from Solar Orbiter at 0.36 au, with other spacecraft providing radio, EUV, and X-ray data from different vantage points. Fortuitously, Solar Orbiter remained magnetically connected to the source throughout, and the ion arrivals were not interrupted by major dropouts and loss of connection, which could have complicated the interpretation (Ho et al. 2022; Mazur et al. 2000). The slope of the ion arrivals (Fig. 2) was slightly lower than the pure velocity dispersion line but implied a length of ~0.38 au, close to the nominal value. The large anisotropies are consistent with minimal scattering in the interplanetary medium. The timing of the type-III emission and particle arrivals is very close – they are simultaneous to within an uncertainty of a few minutes at most for the electrons; the ions also appear to be emitted simultaneously with the electrons, but their longer flight time limits the uncertainties to a few tens of minutes. The spectral forms are typical of many

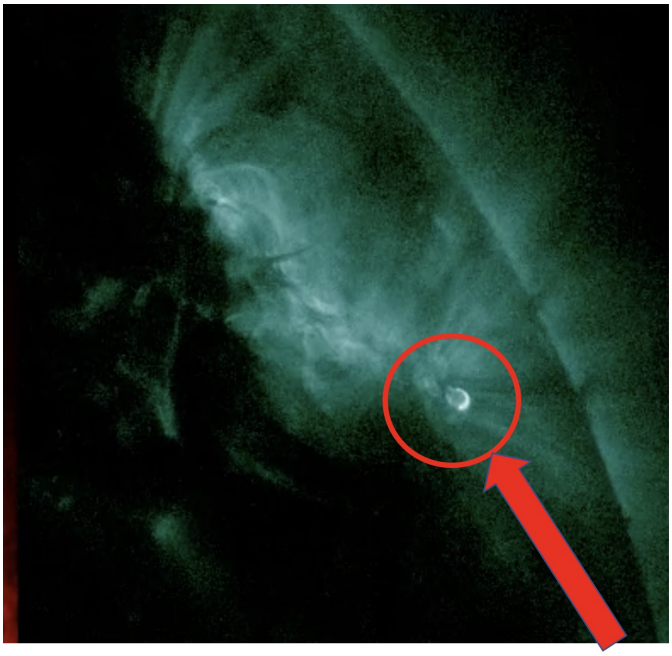

Fig. 4. SDO AIA 94 Å image at 22:15:11 on 18 March 2022 showing a small magnetic loop to the west of AR 12965 that flared in coincidence with the type-III bursts. This image corresponds to event 9 in Figs. 2 and 3. The loop emission was visible for about 4.5 min before fading in this case.

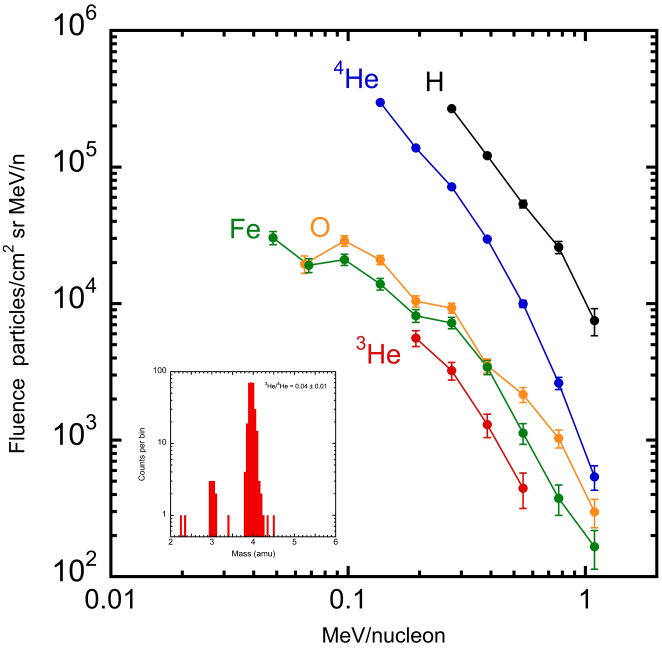

Fig. 5. Energetic particle fluence spectra during event 9 in Fig. 2. The inset histogram shows ^{3}He and ^{4}He over the energy range 0.5–2.0 MeV nucleon^{-1}.

^{3}He-rich events in the range below a few MeV nucleon^{-1}, that is, harder spectra for O and Fe and the ^{3}He:^{4}He ratio increasing with energy (Mason et al. 2002).

A major feature of the observations is the apparent one-to-one association between the type-III bursts and the particle events. It has long been speculated that long periods of ^{3}He enrichments seen at 1 au might be due to the superposition of

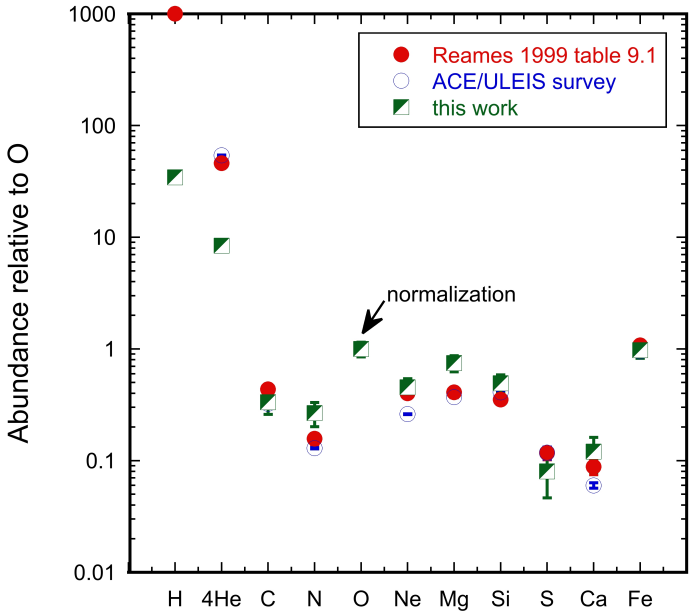

Fig. 6. Ion composition over the range 320–450 keV nucleon^{-1} in event 9 compared with the survey in the same range from ACE/Ultra-Low Energy Isotope Spectrometer (ULEIS) (Mason et al. 2004) and ~2.5 MeV nucleon^{-1} (Reames 1999).

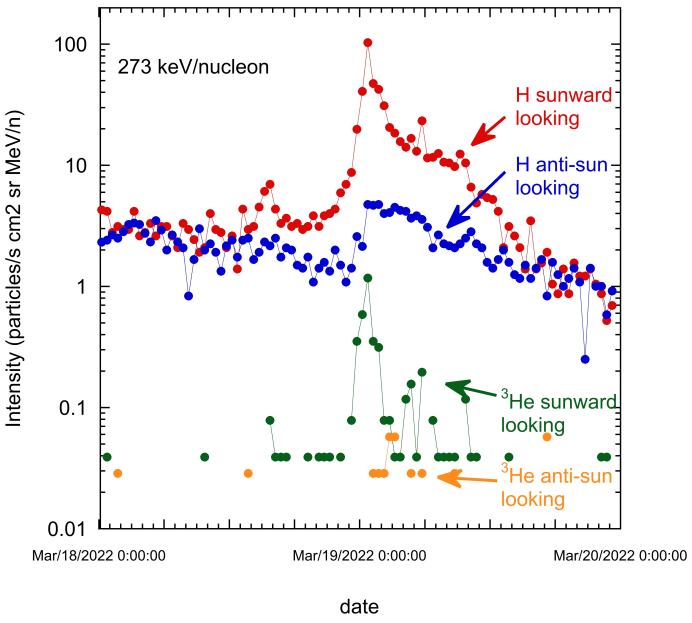

Fig. 7. 30-min-averaged H and ^{3}He intensities from the sunward and anti-sunward SIS telescopes, showing strong anisotropies. Other species showed similar profiles.

multiple events at the Sun (Bučík 2020; Kocharov et al. 2008; Mason 2007), but in this case, using observations closer to the Sun, we argue that each type III is associated with an interplanetary electron- and ^{3}He-rich ion event (see also Bučík et al. 2021). In some cases, faint sources put the particle or radio data near threshold detection, and in one case (event 8) there is a well-detected ion emission with a weak radio source without a clear electron emission. Nevertheless, the bulk of the data points to a one-to-one correspondence. This is not only true when the impulsive SEPs are present, but importantly it is also

the case when the type IIIs are absent before and after the period, when the activity in electrons and heavy ions is extremely low.

The STIX X-ray telescope on Solar Obiter sees small 4–15 keV events in many of the events discussed here, but not all (not shown). The lower panel of Fig. 3 shows some small bumps in near coincidence with the type IIIs, but they are difficult to interpret. During the study period there were eight B- and C-class flares in the NOAA list, but they were of comparatively long duration (~8–10 min and longer), and in the case of the B7.1 event on the NOAA list (Fig. 3 lower panel), AIA movies showed major brightening from AR12965 itself, and not the small loop (Fig. 4).

The small loop flaring in coincidence with the type IIIs is close to the Sun's surface, and given the size of the feature, it seems likely that the particle emission must come from nearby since there is no other apparent activity at the time. Thus, the particles must traverse significant coronal material, which may change their ionization states (Barghouty & Mewaldt 1999; Klecker et al. 2007; Popecki 2006). In that case, the very high temperatures of the flaring loop seen at 94 Å (~7–8 MK) may not be relevant for ionization states (not measured), which, for typical ^{3}He-rich events, are much lower than such high temperatures would imply (Klecker et al. 2006).

The basic features of this series of events are firmly established by the observations presented here: namely, a source near the solar surface associated with a small flaring loop near an AR, with type-III bursts, electrons, and ^{3}He-rich event ions all emitted promptly and in coincidence or close coincidence with the flaring. Alissandrakis et al. (2015) described a small loop near a coronal hole whose flaring in EUV was associated with type-III bursts, seemingly similar to the type-III bursts described here. Wang et al. (2016) presented a survey of ten ^{3}He-rich events observed at 1 au with CME associations and apparently minimal interplanetary scattering, and inferred from the fitted profiles that their set of ion injections started an average of 75±14 min after the electron injections and had durations of 200–550 min. Taken at face value, this is incompatible with the features seen here. Possibly in events with CMEs, the CMEs may play a role, which, along with interplanetary propagation and mixing, account for the differences. Additionally, it has been well established that jets occur in coincidence with ^{3}He-rich events (Bučík et al. 2018a,b; Nitta et al. 2008, 2015; Wang et al. 2006), and there are no obvious jets here. These differences raise the possibilities that the processes that produce the type IIIs and the ^{3}He-rich events may occur in multiple situations in the corona and that the physical mechanisms producing these events are widespread. This is also consistent with the fact that ^{3}He is present in the interplanetary medium 90–100% of the time during solar active periods (Wiedenbeck et al. 2003). In that case, the set of events discussed here may provide important insights into the essential features of the particle acceleration mechanism itself, as opposed to accompanying phenomena that are not actually required.

Acknowledgements. Solar Orbiter is a mission of international cooperation between ESA and NASA, operated by ESA. The Suprathermal Ion Spectrograph (SIS) is a European facility instrument funded by ESA under contract number SOL.ASTR.CON.00004. We thank ESA and NASA for their support of the Solar Orbiter and other missions whose data were used in this letter. Solar Orbiter post-launch work at JHU/APL is supported by NASA contract NNN06AA01C and at CAU by German Space Agency (DLR) grant # 50OT2002. The UAH team acknowledges the financial support by the Spanish Ministerio de Ciencia, Innovacion y Universidades MCIU/AEI Project PID2019-104863RBI00/AEI/10.13039/501100011033. The STIX instrument is an international collaboration between Switzerland, Poland, France, Czech Republic, Germany, Austria, Ireland, and Italy. N.V.N. acknowledges support by NASA grants 80NSSC18K1126 and 80NSSC20K028; R.B. acknowledges support by NASA grants 80NSSC21K1316 and 80NSSC22K0757; V.K. acknowledges support by NASA grants 18-2HSWO218_2-0010 and 19-HSR-19_2-0143. GOES event identifications were from the daily reports prepared by the U.S. Dept. of Commerce, NOAA, Space Weather Prediction Center.

References

Alissandrakis, C. E., Nindos, A., Patsourakos, S., Kontogeorgos, A., & Tsitsipis, P. 2015, A&A, 582, A52
Barghouty, A. F., & Mewaldt, R. A. 1999, ApJS, 520, L127
Bodmer, R., Bochsler, P., Geiss, J., von Steiger, R., & Gloeckler, G. 1995, Space Sci. Rev., 72, 61
Bučík, R. 2020, Space Sci. Rev., 216, 25
Bučík, R., Innes, D. E., Mason, G. M., et al. 2018a, ApJS, 852, 76
Bučík, R., Wiedenbeck, M. E., Mason, G. M., et al. 2018b, ApJ, 869, L21
Bučík, R., Mason, G. M., Gomez-Herrero, R., et al. 2021, A&A, 656, L11
Chollet, E. E., Giacalone, J., Skoug, R. M., Steinberg, J. T., & Gosling, J. T. 2009, ApJS, 705, 1492
Desai, M., & Giacalone, J. 2016, Liv. Rev. Sol. Phys., 13, 3
Gloeckler, G., & Geiss, J. 1998, Space Sci. Rev., 84, 275
Ho, G. C., Mason, G. M., Allen, R. C., et al. 2022, Front. Astron. Space Phys., 9
Klecker, B., Mobius, E., & Popecki, M. A. 2006, Space Sci. Rev., 124, 289
Klecker, B., Mobius, E., & Popecki, M. A. 2007, Space Sci. Rev., 130, 273
Kocharov, L., Laivola, J., Mason, G. M., Didkovsky, L., & Judge, D. L. 2008, ApJS, 176, 497
Krucker, S., Hurford, G. J., Grimm, O., et al. 2020, A&A, 642, A15
Lemen, J. R., Title, A. M., Akin, D. J., et al. 2012, Sol. Phys., 275, 17
Maksimovic, M., Bale, S. D., Chust, T., & Khotyaintsev, Y. 2020, A&A, 642, A12
Mason, G. M. 2007, Space Sci. Rev., 130, 231
Mason, G. M., Dwyer, J. R., & Mazur, J. E. 2000, ApJ, 545, L157
Mason, G. M., Wiedenbeck, M. E., Miller, J. A., et al. 2002, ApJ, 574, 1039
Mason, G. M., Mazur, J. E., Dwyer, J. R., et al. 2004, ApJ, 606, 555
Mazur, J. E., Mason, G. M., Dwyer, J. R., et al. 2000, ApJ, 532, L79
Müller, D., Cyr, O. C. S., Zouganelis, I., Gilbert, H. E., & Marsden, R. 2020, A&A, 642, A1
Nitta, N. V., Mason, G. M., Wiedenbeck, M. E., et al. 2008, ApJ, 675, L125
Nitta, N. V., Mason, G. M., Wang, L., Cohen, C. M. S., & Wiedenbeck, M. E. 2015, ApJS, 806, 235
Popecki, M. A. 2006, Geophys. Monogr., 165, 127
Reames, D. V. 1999, Space Sci Rev, 90, 413
Reames, D. V. 2017, Springer. Lect. Notes Phys., 932
Rodríguez-Pacheco, J., Wimmer-Schweingruber, R. F., Mason, G. M., et al. 2020, A&A, 642, A7
Rouillard, A. P., Pinto, R. F., Vourlidas, A., De Groof, A., & Thompson, W. T. 2020, A&A, 642, A2
Wang, Y.-M., Pick, M., & Mason, G. M. 2006, ApJ, 639, 495
Wang, L., Lin, R. P., Krucker, S., & Mason, G. M. 2012, ApJS, 759, 69
Wang, L., Krucker, S., Mason, G. M., Lin, R. P., & Li, G. 2016, A&A, 585, A119
Wiedenbeck, M. E., Mason, G. M., Christian, E. R., et al. 2003, AIP Conf. Proc., 679, 652
Wimmer-Schweingruber, R. F., Janitzek, N. P., Pacheco, D., et al. 2021, A&A, 656, A22